Available online at www.sciencedirect.com
SCIENCE DIRECT
Polymer 47 (2006) 5117–5123
polymer
www.elsevier.com/locate/polymer

Vibrational dynamics and heat capacity in syndiotactic poly(propylene) form I

Vikal Saxena [a], Ajita Pathak [a], Poonam Tandon [a,*], Vishwambhar Dayal Gupta [a], Mahendra Singh [b]

[a] *Physics Department, Lucknow University, University Road, Lucknow 226 007, Uttar Pradesh, India*
[b] *Physics Department, Brahmanand P.G. College, Kanpur 208004, Uttar Pradesh, India*

Received 1 October 2005; received in revised form 3 May 2006; accepted 4 May 2006
Available online 24 May 2006

Abstract

Normal modes of vibration of syndiotactic polypropylene (sPP) and their dispersion are obtained in the reduced zone scheme for helical form I having the conformational sequence (t_2g_2) using Urey–Bradley force field and Wilson's GF matrix method as modified by Higgs. Optically active frequencies corresponding to the zone center and zone boundary are assigned and characteristic features of the dispersion curves are discussed. In general the dispersion in the helical form is less as compared to the planar form. Heat capacity has been calculated via density-of-states using Debye relation in the temperature range 10–460 K and compared with the experimental measurements.

Keywords: Polypropylene; Syndiotactic form; Dispersion curves

1. Introduction

Syndiotactic polypropylene (sPP) crystallizes at least in three different forms, helical form I, having *ggtt* as a repeat unit is the most common form [1–3], form II has an all trans sequence (*tttt*) [4], and form III conformationally ($t_2g_2t_6g_2$) assumes some of the conformational features of both form I and form II [5]. Here, *g* and *t* denote gauche and trans conformational states, respectively, and the subscript stands for the number of such residues in a repeat unit. The observed spectra of the above two forms are quite different. X-ray studies on oriented fibres of helical sPP have shown that the chain has the conformation of a twofold helix with two monomers per translation repeat unit [6]. In an earlier publication in this journal [7], the authors have reported a study of normal modes and their dispersion for the planar conformation of sPP form II. We report here a similar study on the helical conformation of sPP form I.

In the past decade, a lot of studies have been made on polypeptides and synthetic polymers using infrared (IR) and Raman spectra [8–12]. In general, the IR absorption, Raman spectra, inelastic neutron scattering from polymeric systems are very complex and cannot be unraveled without the full knowledge of dispersion curves. One cannot appreciate without it the origin of both symmetry dependent and symmetry independent spectral features. The physical properties of a polymer are strongly influenced by the conformation of the polymer. Any two polymers, which differ only in the way the repeat units are arranged, would show detectable differences in their spectra. These differences can be used to study both configurational and conformational isomerism in polymers. Infrared and Raman studies on the helical sPP have been reported by several authors [6,13–15]. Schachtschnisder and Snyder [6] have calculated the vibrational frequencies of two forms (form I and form II) of crystalline sPP. Ishioka et al. [13] reported normal mode analysis of form III of sPP. The tacticity of polypropylene has been studied using Raman spectroscopy by Zerbi et al. [14]. Amongst several physico-chemical studies reported recently Hahn et al. [15] have studied the effects of conformational defects on Raman spectra. However, none of them have reported so far on the phonon dispersion, density-of-states and heat capacity as a function of temperature for sPP form I. It is therefore important to carry out a complete normal mode analysis. In this study, we present vibrational dynamics, including the heat capacity of helical sPP.

2. Theory

2.1. Calculation of normal mode frequencies

Normal mode calculation for a polymeric chain was carried out using Wilson's GF matrix method [16] as modified by

* Corresponding author. Tel.: +91 522 2782653; fax: +91 522 2740467.
E-mail address: poonam_tandon@hotmail.com (P. Tandon).

0032-3861/$ - see front matter © 2006 Elsevier Ltd. All rights reserved.
doi:10.1016/j.polymer.2006.05.005

Higgs [17] for an infinite polymeric chain. The vibrational secular equation to be solved is

$$|G(\delta)F(\delta)-\lambda(\delta)I|=0; \quad 0\le\delta\le\pi \tag{1}$$

where δ is the phase difference between the modes of adjacent chemical units, $G(\delta)$ is the inverse kinetic energy matrix and $F(\delta)$ is the force field matrix for a certain phase value. The frequencies ν_i in cm^{-1} are related to eigen values by

$$\lambda_i(\delta)=4\pi^2c^2\nu_i^2(\delta). \tag{2}$$

A plot of $\nu_i(\delta)$ versus δ gives the dispersion curve for the ith mode. The use of the type of force field is generally a matter of one's chemical experience and intuition [18]. In the present work, we have used Urey–Bradley force field [19] that is more comprehensive than valence force field. Recently, spectroscopically effective molecular mechanics model have been used for inter and intra molecular interactions consisting of charges, atomic dipoles and Vander Waals interactions [20].

2.2. Calculation of specific heat

Dispersion curves can be used to calculate the specific heat of a polymeric system. For a one-dimensional system the density of states function or the frequency distribution function expresses the way energy is distributed among the various braches of normal modes in the crystal, specific heat is calculated from the relation

$$g(\nu)=\left[\sum\left(\frac{\partial\nu_j}{\partial\delta}\right)^{-1}\right]_{\nu j(\delta)=\nu j} \tag{3}$$

The sum is over all the branches j. Considering a solid as an assembly of harmonic oscillators, the frequency distribution $g(\nu)$ is equivalent to a partition function. The constant volume heat capacity can be calculated using Debye's relation

$$C_v=\sum g(\nu_j)KN_A\left(\frac{h\nu_j}{KT}\right)^2\left[\frac{\exp(h\nu_j/KT)}{\{\exp(h\nu_j/KT)-1\}^2}\right] \tag{4}$$

with $\int g(\nu_i)d\nu_i=1$.

The constant-volume heat capacity C_v, given by the above equation, can be converted into constant-pressure heat capacity C_p using the Nernst–Lindemann approximation [21]

$$C_p-C_v=3RA_0\left(\frac{C_p^2T}{C_vT_m^0}\right), \tag{5}$$

where A_0 is a constant often of a universal value [3.9×10^{-3} (K mol)/J] and T_m^0 is the estimated equilibrium melting temperature, which is taken to be 460.7 K [22].

3. Results and discussion

A two residue repeat unit (Fig. 1), as in the case of planar sPP [7], is taken which gives rise to 54 dispersion curves. Initially, force constants were transferred from planar sPP [7] and then modified to obtain the 'best fit' to the observed infrared (FT-IR) [6] and Raman spectra [14]. The final force constants along with the internal coordinate are given in Table 1. The force constants given in parenthesis are due to non-bonded interactions. A comparison of the observed and calculated frequencies is given in Tables 2 and 3.

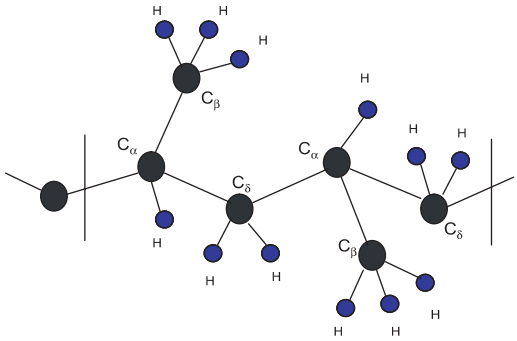

Fig. 1. One chemical repeat unit of sPP form I.

Since the modes above 1400 cm^{-1} are non-dispersive in nature, dispersion curves are plotted in Figs. 2(a) and 3(a) only for the modes below 1400 cm^{-1}. The dispersion curves have four zero frequencies, two at $\delta=0$ and two at $\delta=\pi$; these correspond to the four acoustical modes, three due to translation and one due to chain rotation. For the sake of simplicity, modes are discussed under two heads; dispersive and non-dispersive.

3.1. Non-dispersive modes

All modes above 1400 cm^{-1} are non-dispersive. The assignments of these modes are given in Table 2. These modes are highly localized and are not sensitive to chain conformation.

Table 1
Internal coordinates and Urey–Bradley force constants (md/Å)

Internal coordinates	Force constants
$\nu[C_\beta–H]$	4.200
$\nu[C_\delta–H]$	4.150
$\nu[C_\alpha–H]$	4.360
$\nu[C_\alpha–C_\delta]$	3.400
$\nu[C_\alpha–C_\beta]$	3.700
$\phi[H–C_\delta–H]$	0.370(0.340)
$\phi[H–C_\beta–H]$	0.406(0.295)
$\phi[C_\alpha–C_\delta–H]$	0.490(0.255)
$\phi[C_\delta–C_\alpha–H]$	0.480(0.220)
$\phi[C_\beta–C_\alpha–H]$	0.580(0.210)
$\phi[C_\alpha–C_\beta–H]$	0.365(0.200)
$\phi[C_\alpha–C_\delta–C_\alpha]$	0.790(0.370)
$\phi[C_\delta–C_\alpha–C_\delta]$	0.650(0.270)
$\phi[C_\delta–C_\alpha–C_\beta]$	0.790(0.350)
$\tau[C_\alpha–C_\delta]$	0.008
$\tau[C_\alpha–C_\beta]$	0.009
$\tau[C_\delta–C_\alpha]$	0.008
Off-diagonal interactions	
$\nu[C_\alpha–C_\delta]-\phi[C_\alpha–C_\delta–H]$	0.300
$\nu[C_\alpha–C_\beta]-\phi[C_\beta–C_\alpha–H]$	0.400

Note. ν, ϕ, ω, τ denote stretch, angle bend, wag and torsion, respectively. Stretching force constants between the non-bonded atoms in each angular triplet (gem configuration) are given in parentheses.

Table 2
Non-dispersive modes of sPP

Frequency (cm^{-1})			Assignment (% PED) at $\delta=0$
Calc.	Observed		
	IR[a]	Raman[b]	
2959	2959	2962	$\nu[C_\beta–H](99)$
2959	2959	2962	$\nu[C_\beta–H](99)$
2927	2926	2922	$\nu[C_\delta–H](80)+\nu[C_\alpha–H](19)$
2924	2926	2922	$\nu[C_\delta–H](99)$
2917	2916	2904	$\nu[C_\alpha–H](99)$
2915	2915	2904	$\nu[C_\alpha–H](80)+\nu[C_\delta–H](19)$
2882	2882	2873	$\nu[C_\beta–H](99)$
2882	2882	2873	$\nu[C_\beta–H](100)$
2882	2882	2873	$\nu[C_\beta–H](99)$
2882	2882	2873	$\nu[C_\beta–H](99)$
2857	2843	2840	$\nu[C_\delta–H](99)$
2856	2843	2840	$\nu[C_\delta–H](99)$
1465	1465	1466	$\phi[H–C_\beta–H](95)$
1465	1465	1466	$\phi[H–C_\beta–H](94)$
1465	1463	1466	$\phi[H–C_\beta–H](95)$
1465	1463	1466	$\phi[H–C_\beta–H](94)$
1442	1432	1445	$\phi[H–C_\delta–H](71)+\phi[C_\alpha–C_\delta–H](19)$
1453	1455	1445	$\phi[H–C_\delta–H](76)+\phi[C_\alpha–C_\delta–H](20)$
1384	1379	–	$\phi[H–C_\beta–H](35)+\phi[C_\alpha–C_\beta–H](31)+\nu[C_\alpha–C_\beta](19)$
1383	1348	–	$\phi[H–C_\beta–H](28)+\phi[C_\alpha–C_\beta–H](26)+\nu[C_\alpha–C_\beta](19)$
1375	1373	1374	$\phi[C_\delta–C_\alpha–H](27)+\nu[C_\alpha–C_\delta](18)+\phi[H–C_\beta–H](16)+\phi[C_\alpha–C_\beta–H](15)$
1319	1311	1312	$\phi[C_\beta–C_\alpha–H](30)+\phi[C_\alpha–C_\delta–H](27)+\nu[C_\alpha–C_\delta](12)+\phi[C_\delta–C_\alpha–H](11)$
1299	1293	1296	$\phi[C_\delta–C_\alpha–H](23)+\phi[C_\alpha–C_\delta–H](23)+\phi[C_\beta–C_\alpha–H](20)+\nu[C_\alpha–C_\delta](15)$
1253	1264	1263	$\phi[C_\alpha–C_\delta–H](77)$
876	870	872	$\phi[C_\alpha–C_\beta–H](78)+\nu[C_\alpha–C_\delta](11)$
861	867	871	$\phi[C_\alpha–C_\beta–H](47)+\nu[C_\alpha–C_\delta](26)+\phi[C_\alpha–C_\delta–H](13)$
858	–	–	$\phi[C_\alpha–C_\beta–H](72)+\nu[C_\alpha–C_\delta](12)$
849	–	844	$\phi[C_\alpha–C_\delta–H](49)+\phi[C_\alpha–C_\beta–H](41)$
210	–	202	$\tau[C_\alpha–C_\beta](96)$
208	–	204	$\tau[C_\alpha–C_\beta](91)$
176	–	172	$\phi[C_\alpha–C_\delta–C_\alpha](49)+\phi[C_\delta–C_\alpha–C_\beta](27)$
63	–	62	$\tau[C_\alpha–C_\delta](38)+\phi[C_\delta–C_\alpha–C_\delta](28)+\phi[C_\alpha–C_\delta–C_\alpha](16)$
61	–	62	$\tau[C_\delta–C_\alpha](56)+\tau[C_\alpha–C_\delta](20)$

[a] Ref. [6].
[b] Ref. [14].

The calculated frequencies in the C–H stretching region from 3100 to 2800 cm^{-1} are in good agreement with the observed bands. The asymmetric stretch modes of methyl group have been matched to the peak at 2959/2962 cm^{-1} in IR/Raman spectra. The symmetric stretches of methyl group are calculated at 2882 cm^{-1} and matched at 2882/2873 cm^{-1} in IR/Raman spectra. The degenerate asymmetric stretch of methylene group is calculated and assigned to the peak at same frequencies in IR/Raman spectra. The symmetric stretch of methylene group is calculated at 2856 cm^{-1} and assigned to the peak at 2843/2840 cm^{-1} in IR/Raman spectra. The C_α–H stretch is calculated at 2917 cm^{-1} corresponding to the observed peak at 2916/2904 cm^{-1} in IR/Raman spectra. The region from 1380 to 1470 cm^{-1} contains bending modes of the methyl group and scissoring modes of the methylene group. The calculated frequencies in this region fit well with the observed data. The potential energy distribution shows that CH_3 symmetric bend mixes with side chain C_α–C_β stretch. The dispersion curves are essentially flat in this region. The bands in the region 1300–1370 cm^{-1} correspond to C_α–H bending and CH_2 wag modes. The C_α–H bend calculated at 1375 cm^{-1} and assigned to the peak at the 1373 cm^{-1} has 18% contribution from backbone C_α–C_δ stretch vibration. The other mode at 1319 cm^{-1} is a mixture of C_α–H bend and CH_2 wag. Both of these modes are non-dispersive. The modes at 1299 and 1253 cm^{-1} also have a little dispersion. The major contribution of –CH_2 wag is contained in the calculated mode at 1253 cm^{-1}.

Methyl rocking modes calculated at 876 cm^{-1} and 861 cm^{-1} at $\delta=0$ are assigned to the observed peak at 870/872 cm^{-1} and 867/871 in IR/Raman spectra, respectively. These modes are mixed with side chain C_α–C_β stretch and are non-dispersive.

A comparison of modes of planar sPP with helical sPP and iPP (Table 4) indicates that most of the non-dispersive modes are well localized and not much affected by change in configuration and conformation of PP chain. Some modes such as 210,176 and 63 cm^{-1} C_α–C_β torsions, C–C–C backbone bending and C_α–C_δ torsions, respectively, show negligible dispersions but some other modes, which appear at the zone center at 63 and 61 cm^{-1} go through dispersive behavior. Because of the coupling these modes lose their local character (specially torsion mode) and spread to neighbouring units as well. These modes have been observed in Raman spectra.

3.2. Dispersive modes

The modes, which are dispersive, are mixed modes that are highly coupled along the chain. These modes at the zone center and zone boundary along with their assignments are given in Table 3. An interesting feature of the dispersive modes of sPP form II [7] is their tendency to bunch towards the zone boundary. Such a situation is not observed in helical form of sPP.

The mode at 1338 cm^{-1} is a mixed mode corresponding to the observed peak at 1332/1331 cm^{-1} in IR/Raman spectra. It has mixed contribution of C_α–H bend, C_α–C_δ stretch and CH_2 wag. This mode disperses by 21 wave number and is calculated at 1359 cm^{-1} at the zone boundary The CH_2 twisting mode calculated at 1203 cm^{-1} at the zone center is assigned to the observed peak at 1202/1205 cm^{-1} in IR/Raman spectra. The energy of this mode increases with increase in δ and reaches at 1217 cm^{-1} near the zone boundary. The mode calculated at 1242 cm^{-1} has exactly the same frequency as observed in the IR and Raman and has been assigned to the phonon $\{\phi[C_\alpha–C_\delta–H]+\phi[C_\delta–C_\alpha–H]+\nu[C_\alpha–C_\delta]\}$ calculated at 1236 cm^{-1}.

For modes between 1400 and 830 cm^{-1} there is practically no change in the dispersive features for both helical and planar conformations of sPP except that the amount of dispersion in helical sPP is less. For example, the skeletal modes calculated at 1124 and 1084 cm^{-1} approach 1135 and 1069 cm^{-1},

Table 3
All dispersive modes in sPP

Frequency (cm^{-1})			Assignment (%PED) at $\delta=0$	Frequency (cm^{-1})			Assignment (%PED) at $\delta=\pi$
Calc.	Observed			Calc.	Observed		
	IR[a]	Raman[b]			IR[a]	Raman[b]	
1338	1332	1331	ϕ[C_δ–C_α–H](28)+ν[C_α–C_δ](26)+ϕ[C_α–C_δ–H](15)+ϕ[C_β–C_α–H](10)	1359	1360	1360	ϕ[C_δ–C_α–H](36)+ν[C_α–C_δ](26)+ϕ[C_α–C_δ–H](14)
1246	1242	1242	ϕ[C_α–C_δ–H](65)+ϕ[C_δ–C_α–H](14)+ν[C_α–C_δ](11)	1234	–	–	ϕ[C_α–C_δ–H](50)+ϕ[C_β–C_α–H](24)+ϕ[C_δ–C_α–H](13)
1236	–	1242	ϕ[C_α–C_δ–H](47)+ϕ[C_β–C_α–H](22)+ϕ[C_δ–C_α–H](14)	1219	–	–	ϕ[C_α–C_δ–H](78)+ϕ[C_δ–C_α–H](10)
1203	1202	1205	ϕ[C_α–C_δ–H](44)+ϕ[C_β–C_α–H](21)+ϕ[C_δ–C_α–H](17)	1217	–	1205	ϕ[C_α–C_δ–H](77)
1140	1153	1153	ϕ[C_α–C_δ–H](37)+ν[C_α–C_δ](21)+ν[C_α–C_β](13)	1171	1167	1168	ν[C_α–C_δ](33)+ϕ[C_α–C_δ–H](11)+ν[C_α–C_β](11)+ϕ[C_δ–C_α–C_δ](10)
1124	–	1106	ν[C_α–C_δ](28)+ν[C_α–C_β](22)+ϕ[C_δ–C_α–H](18)+ϕ[C_α–C_δ–H](12)	1135	–	1153	ϕ[C_δ–C_α–H](23)+ν[C_α–C_β](22)+ν[C_α–C_δ](15)+ϕ[C_α–C_δ–H](13)
1084	1088	1088	ν[C_α–C_δ](53)+ϕ[C_δ–C_α–H](15)+ϕ[C_α–C_δ–H](15)	1069	1060	1060	ν[C_α-C_δ](56)+ϕ[C_δ-C_α-H](25)
1034	1035	1039	ν[C_α–C_δ](38)+ϕ[C_α–C_δ–H](28)+ϕ[C_α–C_β–H](11)	1019	1035	1039	ν[C_α–C_δ](58)+ϕ[C_α–C_δ–H](17)+ϕ[C_α–C_β–H](11)
977	976	978	ϕ[C_α–C_β–H](23)+ν[C_α–C_δ](21)+ν[C_α–C_β](20)+ϕ[C_α–C_δ–H](10)	984	977	978	ν[C_α–C_β](38)+ϕ[C_α–C_δ–H](21)+ϕ[C_α–C_β–H](15)
844	–	–	ϕ[C_α–C_β–H](76)+ν[C_α–C_δ](10)	826	–	825	ϕ[C_α–C_δ–H](62)+ν[C_α–C_β](11)
823	812	825	ϕ[C_α–C_δ–H](64)+ν[C_α–C_β](20)	809	812	812	ϕ[C_α–C_δ–H](62)+ν[C_α–C_δ](17)
531	535	535	ϕ[C_α–C_δ–C_α](32)+ϕ[C_δ–C_α–C_β](25)+ν[C_α–C_β](12)	547	535	550	ϕ[C_δ–C_α–C_β](48)+ϕ[C_α–C_δ–C_α](21)
451	–	462	ϕ[C_δ–C_α–C_β](26)+ϕ[C_δ–C_α–H](20)+ϕ[C_δ–C_α–C_δ](19)+ϕ[C_α–C_δ–H](11)	464	468	462	ϕ[C_δ–C_α–C_δ](39)+ϕ[C_α–C_δ–C_α](24)+ν[C_α–C_β](11)
418	–	424	ϕ[C_δ–C_α–C_β](81)	436	–	429	ϕ[C_δ–C_α–C_β](40)+ϕ[C_δ–C_α–H](14)+ϕ[C_δ–C_α–C_δ](12)+ϕ[C_β–C_α–H](10)
342	344	–	ϕ[C_δ–C_α–C_δ](39)+ϕ[C_δ–C_α–C_β](34)	412	–	398	ϕ[C_δ–C_α–C_β](52)+ϕ[C_δ–C_α–H](16)
342	–	–	ϕ[C_δ–C_α–C_β](44)+ϕ[C_δ–C_α–C_δ](18)+ϕ[C_δ–C_α–H](11)+ϕ[C_α–C_δ–C_α](10)	272	–	292	ϕ[C_δ–C_α–C_β](69)+ν[C_α–C_δ](12)
306	–	312	ϕ[C_δ–C_α–C_β](35)+ν[C_α–C_δ](26)+ϕ[C_α–C_δ–C_α](12)	253	–	260	ϕ[C_δ–C_α–C_δ](42)+τ[C_α–C_β](19)+ϕ[C_δ–C_α–C_β](15)
73	–	62	τ[C_δ–C_α](43)+τ[C_α–C_δ](42)	169	–	172	ϕ[C_α–C_δ–C_α](33)+ϕ[C_δ–C_α–C_β](16)+ϕ[C_δ–C_α–C_δ](16)+τ[C_α–C_δ](11)

[a] Ref. [6].
[b] Ref. [14].

respectively, at $\delta=\pi$. However, for the planar zig-zag backbone of sPP [7] these modes show a steeper dispersion; both the modes at 1158 and 1121 cm^{-1} ($\delta=0$) frequencies converges to 1103 cm^{-1}, respectively, at $\delta=\pi$. The larger meandering of the dispersion curves in planar form is indicative of a relatively more sensitive coupling between the successive units in planar form as compared with the helical sPP.

The calculated frequency at 823 cm^{-1} with major contribution from CH_2 rocking matches well with the observed frequency at 812/825 cm^{-1} in IR/Raman spectra. This mode is observed at 812 cm^{-1} in helical sPP [15] and it is very sensitive to backbone conformation. It shifts to 832 cm^{-1} in planar sPP [23].

The modes below 600 cm^{-1} show large dispersion. The mode calculated at 531 cm^{-1} at $\delta=0$ and observed at 535 cm^{-1} in Raman has major contributions from the angle bends C_α–C_δ–C_α, C_δ–C_α–C_β beyond $\delta=40\pi$ the contribution of C_δ–C_α–C_β increases and reaches at 547 cm^{-1} near zone boundary. Similar behavior is exhibited by the modes calculated at 451 and 418 cm^{-1}. The phenomena of bunching at $\delta=0$ is observed for the mode calculated at 342 cm^{-1}. On increasing the δ value, this mode calculated at 342 cm^{-1} starts dispersion and its two branches are calculated at 412 and 272 cm^{-1} with entirely different contributions near zone boundary.

The lower-frequency modes are more sensitive to chain structure and show relatively better dispersion. The entirely different dispersion features in helical sPP for the lower frequency region, especially the acoustic modes, are characteristic of the twofold helical chain symmetry. The two acoustic branches in the dispersion curves are similar in shape to the dispersion of these branches in other twofold helical polymers such as polyethylene [8], polyglycine I [12], polystyrene [24], etc.

Comparison of the modes for sPP (all trans), sPP (helical) and iPP is shown in Table 4. The CH_2 wag, CH_3 rock and backbone C–C stretch and side chain C–C stretch. These three forms and skeletal deformation modes have large differences. These modes involve large coupling and are mixed with each other. The difference in the observed frequencies arises mainly because of the placement of the side group in different lateral

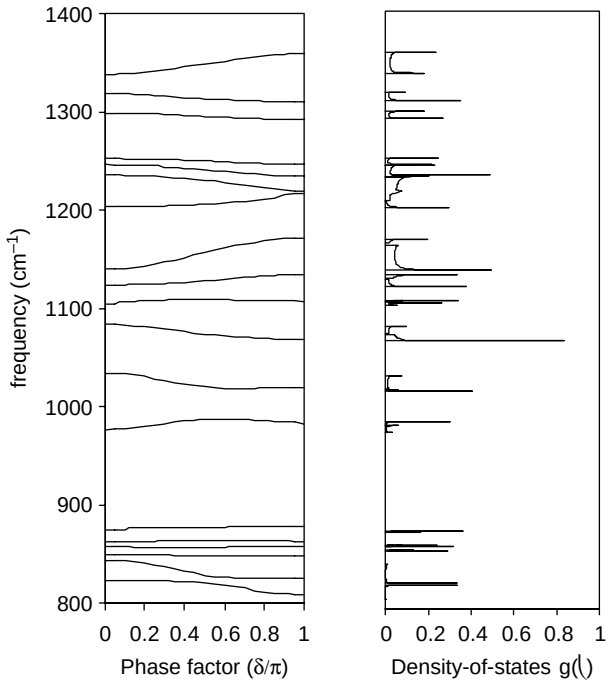

Fig. 2. (a) Dispersion curves of sPP form I (1400–800 cm^{-1}). (b) Density-of-states of sPP form I (1400–800 cm^{-1}).

positions, which in turn brings about the change in interaction constants, which are responsible for the frequency shifts.

The characteristic features of the polymer under study have been related to its vibrational spectra and compared with the results reported earlier by us [7] and Takeuchi [26]. Both, the dispersive nature and conformational sensitivity of the spectra lie in the region of skeletal deformation (C_α–C_δ–C_α) and

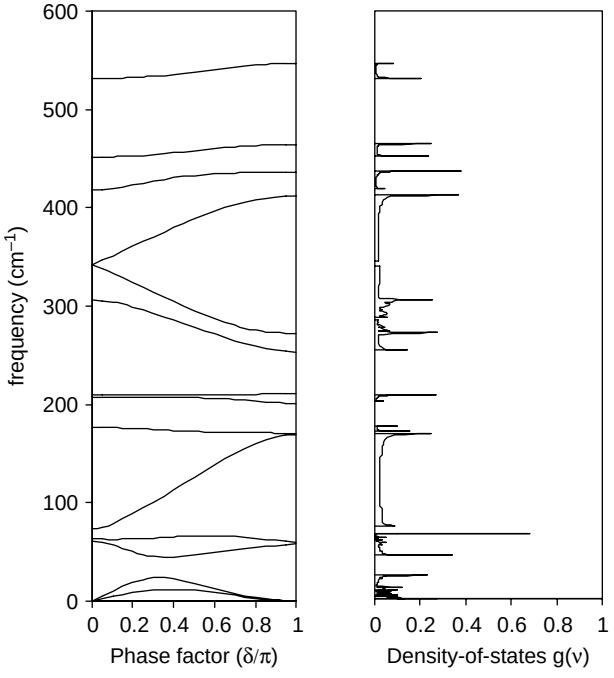

Fig. 3. (a) Dispersion curves of sPP form I below 600 cm^{-1}. (b) Density-of-states of sPP form I below 600 cm^{-1}.

Table 4
Comparison of modes of sPP (all trans), sPP (helical) and iPP

Assignments	Frequency (cm^{-1})			
	sPP all trans observed IR[a]	sPP helical observed		IPP observed IR[b]
		IR[a]	Raman[c]	
CH_3 asymmetric stretch	2959	2959	2962	2956
CH_3 symmetric stretch	2880	2882	2873	2880
CH stretch	2916, 2905	2915	2904	2907
CH_2 asymmetric stretch	2926	2927	2922	2925
CH_2 symmetric stretch	2856[d]	2843	2840	2868
CH_3 asymmetric deformation	1466	1465	1466	1459
CH_2 scissoring	1455, 1450	1432, 1455	1445	1454
CH_3 symmetric deformation	1381	1379	–	1377, 1359
CH_2 wag	1350	1287,1346	1374	1378, 1305
CH_2 twist	1200, 1226	1234[e], 1202	1242, 1202	1219, 1239
CH_2 rock	831, 829[e]	842, 812	844, 825	841, 807
CH_3 rock	972, 867	977[e], 870	978, 871	997, 973
CH bending	1322	1332	1331	1329
C–C stretch (backbone)	1154, 1095	1153, 1035	1153, 1039	1167, 1153
C–C stretch (sidechain)	1130	906, 1005[e]	–	1103, 1044
C–C–C bending	492	535, 483, 468	535,462,424	452

[a] Ref. [6].
[b] Ref. [25].
[c] Ref. [14].
[d] Only calculated modes are known.
[e] Ref. [23].

torsion (C_α–C_β), (C_β–C_α) (below 600 cm^{-1}). These characteristics of conformational mode are reflected in the meandering of the dispersion curves over the entire chain. In case of PP its variation from form I to II reflects the change in syndiotacticity. For example, in the sPP form I (C_α–C_δ–C_α) bending appears at 531 cm^{-1} ($\delta = 0$) and 547 cm^{-1} ($\delta = \pi$) but it shifts to 495 and 450 cm^{-1}, respectively, in form II. Similar shifts are observed in isotactic form. The exact magnitude of the shifts depends on the compactness of the helix. These results are shown in Table 5.

3.3. Frequency distribution function and heat capacity

A study of the dispersion curves is important to appreciate the origin of symmetry dependent and symmetry independent spectral features. It also enables the calculation of frequency distribution function. The frequency distribution function (density-of-states) shows how the energy is distributed among the various branches of the normal modes. Figs. 2(b) and 3(b) show the plots of density-of-states versus frequency as obtained from the dispersion curves. The peaks of the frequency distribution curves correspond to regions of high density-of-states (Von Hove type singularities).

Table 5
Some characteristic modes of polypropylene

Assignments	Calculated frequency (cm^{-1})					
	sPP all trans		sPP helical		iPP	
	At $\delta=0$	At $\delta=\pi$	At $\delta=0$	At $\delta=\pi$	At $\delta=0$	At $\delta=\pi$
C–C stretch (backbone)	1093	1085	1084	1069	–	–
C–C stretch (sidechain)	1121	1103	1124	1135	–	–
C_α–C_δ–C_α bending	495	450	531	547	473	509
C_α–C_δ–C_β bending	427	450	451	464	391	445
$\tau(C_\alpha$–$C_\delta)$	–	65	73	169	–	90
$\tau(C_\alpha$–$C_\delta)$	–	58	61	61	–	58
$\tau(C_\alpha$–$C_\beta)$	196	196	210	211	203	207

The frequency distribution function can also be used to calculate the thermodynamical properties such as heat capacity, enthalpy changes, etc. It has been used to obtain the heat capacity as a function of temperature. We have calculated the heat capacity of sPP in the temperature range 10–460 K using Debye's equation. The variation of heat capacity with temperature as obtained from the density-of-states according to equation number 4 is shown in Fig. 4. The calculated heat capacity data is shown to be in agreement with the experimental measurements as obtained from ATHAS data bank when reduced to the results for a single monomeric residue per unit. The initial disagreement is mainly because of the absence of lattice modes in our calculation. These modes fall in the low frequency region and heat capacity is sensitive in these modes. Beyond 295 K, the divergence between the two curves is because of the glass transition in syndiotactic polymers and at this temperature the polymer goes in to rubbery state. The possible reason for deviation from experimental curve could be because the authors have not mentioned about the tactic nature of the sample whether it is isotactic, syndiotactic and atactic or a mixture of these states. Lack of this information makes our comparison of calculated and measured heat capacities as a function of temperature somewhat limited. It is true that comparison of calculated and measured heat capacities as a function of temperature would have been more meaningful if the authors [22] had mentioned the percentage of crystallinity in this sample. However, they have not given any such information. We therefore, presume that the sample is 100% crystalline. Further, we feel that the agreement between the calculated and measured heat capacities would become even better if a certain percent of the sample existed in amorphous state. Such a sample would make lesser contribution in the low frequency region because the heat capacities are sensitive to lattice and chain modes, which occur in this frequency region. This missing contribution when compensated for in 100% crystallinity will push the two curves (theoretical and experimental) closer in the low frequency region before the glass transition.

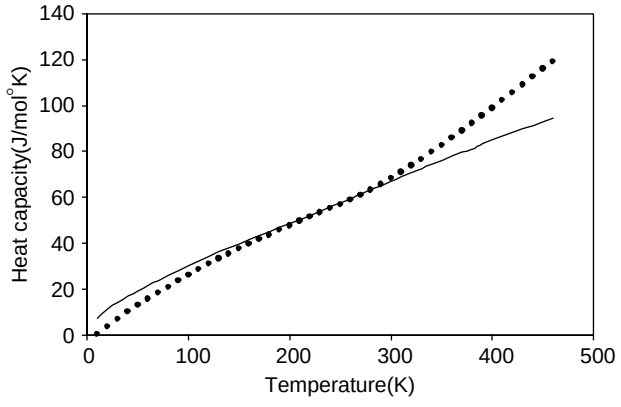

Fig. 4. Variation of heat capacity of sPP form I as a function of temperature. Solid line represents the theoretical values and (●) represents the experimental data.

4. Conclusion

All characteristic features of the dispersion curves such as regions of high density of states convergence and divergence of modes near the zone center/boundary have been well interpreted from the vibrational dynamics of syndiotactic polypropylene. A comparison is made with the spectra of its isotactic and helical form to identify the conformational sensitive modes. In addition, the heat capacity as a function of temperature in the region 10–460 K has been successfully explained.

References

[1] Cording P, Natta G, Ganis P, Temuussi PA. J Polym Sci, Part C 1967;16:2477.
[2] Rosa CD, Corradini P. Macromolecules 1993;26:5711.
[3] Auriemma F, Rosa CD, Corradini P. Macromolecules 1993;26:5719.
[4] Chatani Y, Maruyama H, Noguchi K, Asanuma T, Shiomura T. J Polym Sci, Polym Lett 1990;28:393.
[5] Chatani Y, Maruyama H, Noguchi K, Asanuma T, Shiomura T. J Polym Sci, Polym Phys Ed 1991;29:1649.
[6] Schachtschnisder JH, Snyder RG. Spectrochim Acta 1965;21:1527.
[7] Saxena V, Misra RM, Tandon P, Gupta VD. Polymer 2005;46:7386–93.
[8] Tasumi M, Shimanouchi T. J Mol Spectrosc 1962;9:261.
[9] Pande S, Kumar A, Tandon P, Gupta VD. Vibr Spectrosc 2001;26:161.
[10] Pande S, Tandon P, Gupta VD. J Macromol Sci (Phys) 2002;41(1):1.
[11] Arjunan V, Subramanian S, Mohan S. Spectochim Acta, Part B 2001;57:2547.
[12] Gupta VD, Trevino S, Boutin H. J Chem Phys 1968;48:3008.
[13] Ishioka T, Masaoka N. Polymer 2002;43:4639.
[14] Masetti G, Cabassi F, Zerbi G. Polymer 1980;21.
[15] Hahn T, Suen W, Kang S, Hsu SL, Stidhou HD, Siedle AR. Polymer 2001;42:5813.

[16] Wilson EB, Decius JC, cross PC. Moleculer vibrations: the theory of infrared and Raman vibration spactra. New York: Dover publications; 1980.
[17] Higgs PW. Proc R Soc (London) 1953;A220:472.
[18] Mannfors B, Palmo K, Krimm S. J Mol Struct 2000;556:1.
[19] Urey HC, Bradley HC. Phys Rev 1931;38:1969.
[20] Qian W, Mirikin NG, Krimm S. Chem Phys Lett 1999;315:125.
[21] Pan R, Verma-Nair M, Wunderlich B. J Therm Anal 1989;35:955.
[22] ATHAS DATABANK, 1993.
[23] Nakaoki T, Yamanaka T, Ohira Y, Horii F. Macromolecules 2000;33:2718.
[24] Rastogi S, Gupta VD. J Macromol Sci 1995;B34(1/2):1–13.
[25] Tadokaro H, Kobayashi M, Ukita M, Yasupuku K, Murahashi S. J Chem Phys 1965;42:4.
[26] Takeuchi H, Higgins JJ, Hill A, Mocanachi A, Allen G, Sterling GC. Polymer 1982;23:499.